Digest Journal of Nanomaterials and Biostructures Vol. 18, No. 4, October-December 2023, p. 1147-1158

Facile synthesis of N-doped TiO_2 nanosheets with exposed (001) facets for enhancing photocatalytic activity

Y. Sun[a,b], Y. Zhong[a], X. Luo[a], Y. J. Duan[a], K. Lei[a], L. J. Mao[a], W. Feng[a,b,*]
[a]*School of Mechanical Engineering, Chengdu University, Chengdu, 610106, China*
[b]*Sichuan Province Engineering Technology Research Center of Powder Metallurgy, Chengdu, 610106, China*

Nitrogen-doped TiO_2 with exposed (001) facets was prepared by hydrothermal method using TiN as precursor. The effect of the proportion of HF and HCl on the crystal structure, morphology, optical properties and photocatalytic activity were investigated. The photocatalytic performance of N-doped TiO_2 nanosheets was evaluated by the degradation of methylene blue (MB) under xenon lamp light source. The results showed that TiO_2 demonstrated nanorod structure with a single rutile phase in the absence of HF while anatase TiO_2 exhibited nanosheet structure with exposed (001) facets in the presence of HF. With the increase of HF addition, the degradation rate of the N-doped TiO_2 decreased gradually. When the addition of HF was 1 mL, TiO_2 showed the highest photocatalytic activity, which was mainly attributed to the large specific surface area and optimal percentage of exposed (001) facets.

(Received July 17, 2023; Accepted September 25, 2023)

Keywords: N-doped TiO_2, Nanosheets, (001) facets, Photocatalytic

1. Introduction

TiO_2 has been known as one of the best photocatalysts due to its unique properties, such as chemical stability, non-toxicity, and low cost, which is widely applied in photocatalytic degradation of organic pollutants, hydrogen production, self-cleaning glass and solar cells [1-4]. However, the large bandgap (3.2 eV) of anatase TiO_2 with low utilization of sunlight and fast recombination of photogenerated electron-hole pairs greatly limit its practical application [5-7]. Recently, many researchers [8-11] focus on improving activity of TiO_2 through controlling the growth process of TiO_2 with exposed facets，which has been regarded as a promising strategy to tune the charge separation and charge-involving chemical reactions [12]. It is well known that during the crystal growth of anatase TiO_2, the most exposed facets are (101) facets with a low surface energy (0.44 J/m^2) and poor activity [13]. Since Yang et al. [14] first synthesized single crystal anatase TiO_2 sheets with 47% (001) facets of a higher surface energy (0.90 J/m^2), several research groups have attempted to increase the ratio of exposed (001) facets, which is beneficial to enhance the photocatalytic activity of TiO_2. Among these reports [15-19], anatase TiO_2 with exposed (001) facets can be synthesized using $Ti(OBu)_4$, TiF, TiO_2 powder, Ti powder, Ti foil as raw materials and HF as a capping agent, which may have no visible light response.

* Corresponding author: fengwei@cdu.edu.cn
https://doi.org/10.15251/DJNB.2023.184.1147

To enhance visible light absorption of TiO_2, in this work, N-doped TiO_2 nanosheets with exposed (001) facets were synthesized by a facile route of one-step hydrothermal method without any calcining, employing TiN as precursor. Moreover, according to the previous literatures [20-22], fluorine plays an important role in the growth of anatase TiO_2 while chlorine promotes the growth of rutile TiO_2. To our best knowledge, there are few reports on the combined action of F^- and Cl^- during the hydrothermal process. Herein, using TiN as titanium source, the crystal structure and size of N-doped TiO_2 nanosheets were controlled through adjusting the proportion of HCl and HF addition. The effect of F ions ratio on the crystal structure, morphology, surface area, absorption ability and photocatalytic activity of TiO_2 nanosheets were systematically investigated.

2. Experimental

2.1. Preparation

The N-doped TiO_2 samples were prepared by hydrothermal method using nano titanium nitride (Aladdin) as precursor. In a typical synthesis, 1.8 g of TiN powder were dispersed in 26 mL deionized water, followed by adding different volume ratios of HF and HCl (shown in Table 1) with continuous stirring for 30 min. The mixture was transferred into a 50 mL Teflon-lined stainless autoclave and heated at 200 ℃ for 18 h. After cooling down to room temperature, the product was centrifugation and washed with deionized water and ethanol for several times. Finally, the N-doped TiO_2 samples prepared with different HF additions (1, 2, 3 mL) were obtained by drying in an oven at 80 ℃, which were labeled as TF1, TF2, TF3, respectively. For comparison, TiO_2 samples were also hydrothermally synthesized without HF or HCl, and labeled as TF0 and TF4, respectively.

2.2. Characterization

Crystal structure of the samples was characterized by X-ray diffractometer (XRD, DX-2700B) with Cu Kα radiation. The surface morphology and microstructure of the samples were measured using a scanning electron microscope (FESEM, SU8220, Hitachi) and a high-resolution transmission electron microscope (HRTEM, Tecnai G2 F20, FEI). The chemical state and XPS valence band were detected by X-ray photoelectron spectroscopy (XPS, ESCALAB Xi+, Thermo Fisher Scientific). The Brunauer-Emmett-Teller (BET) surface area was determined using a nitrogen adsorption apparatus (V-sorb 2800P, Gold APP). UV-vis diffuse reflectance spectra (DRS) were recorded on a UV-Vis spectrophotometer (UV-3600, Shimadzu) using $BaSO_4$ as reference material. Photoluminescence (PL) emission spectra were analyzed using a fluorescence spectrophotometer (F-4600, Hitachi) with excitation wavelength of 300 nm.

2.3. Photocatalytic activity test

The photocatalytic properties of the N-doped TiO_2 nanosheets were evaluated by measuring the degradation of methylene blue (MB) with a 350 W xenon lamp. 0.2 g of photocatalyst was added into 100 mL MB aqueous solution with an initial concentration of 10 mg/L and then ultrasonic dispersed uniformly. Before irradiation, the mixed solution was stirred continuously in the dark for 30 min to reach adsorption-desorption equilibrium. Then 4 mL of suspension solution was taken out from the reactor at every 30 min interval during the irradiation.

After centrifugation, The MB concentration was determined by a UV-vis spectrophotometer (UV-6100A, Shanghai Metash).

3. Results and discussion

3.1. XRD analysis

The XRD patterns of TiO_2 derived from the TiN precursor with different proportions of HF and HCl are shown in Fig. 1. It is clear that the TiN precursor exhibits cubic phase and no TiN can be observer after hydrothermal process, indicating TiN precursor has been oxidized completely. Furthermore, all TiO_2 samples display well-crystallized structure without calcining. As shown in Fig. 1, TiO_2 samples are pure anatase phase (JCPDS No. 21-1272) in the presence of HF. With increasing addition of HF, the intensity of diffraction peaks become stronger and sharper, which is ascribed to the fact that fluorine ions could improve the crystallinity of anatase TiO_2 [23]. Additionally, all peaks of TF0 sample are assigned to rutile phase (JCPDS No. 21-1276) in the presence of HCl alone, which is in good agreement with previous report [24]. The average crystalline size of TiO_2 can be calculated by Scherrer formula [25] and the results are listed in Table 1. The crystalline size of rutile phase is larger than that of anatase phase. Particularly, the crystalline size of anatase TiO_2 nanosheets increases with the increasing ratio of HF. This result is consistent with previous report that surface fluorination and an acidic synthesis condition can enhance the growth and crystallization of TiO_2 [26].

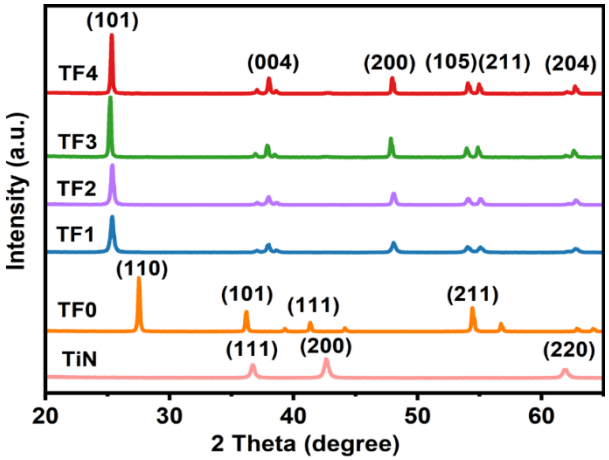

Fig. 1. XRD patterns of TiN powder and TiO_2 prepared by different HF additions.

Table 1. The crystalline size of different samples.

Sample	V_{HF} (mL)	V_{HCl} (mL)	Phase	Crystalline size (nm)
TF0	0	4	Rutile	45.96
TF1	1	3	Anatase	27.48
TF2	2	2	Anatase	31.70
TF3	3	1	Anatase	43.75
TF4	4	0	Anatase	46.28

3.2. Morphology characterization

Fig. 2 shows the SEM images of TiN precursor and synthesized TiO_2 samples. As shown in Fig. 2a, the purchased TiN precursor is nanoparticles with a particle size of about 25 nm. When TiO_2 was prepared in the absence of HF, TF0 sample (Fig. 2b) demonstrates nanorod structure, which is mainly attributed to the fact that HCl can promote the formation of rutile TiO_2 nanorods [27]. Different from the growth of TiO_2 nanorods, with the addition of HF, anatase TiO_2 samples (Fig. 2 c-f) show a typical structure composed of a large number of uniform nanosheets. Obviously, the particle size of TiO_2 increases with the increase of HF. Meanwhile, the side length and the sheet thickness of nanosheets increase.

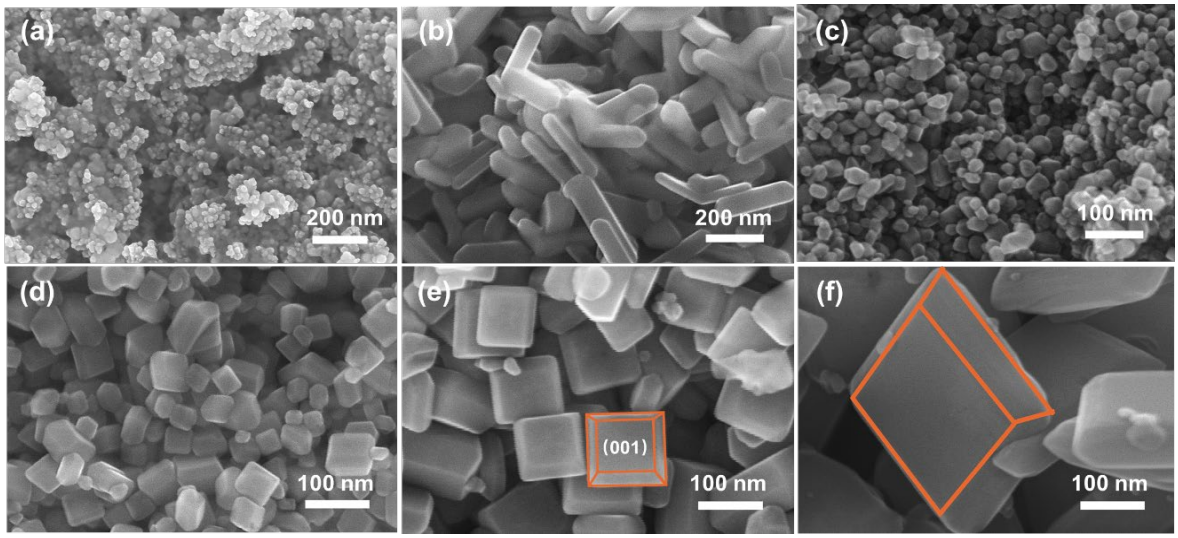

Fig. 2. SEM images of the prepared samples: (a) TiN, (b) TF0, (c) TF1, (d) TF2, (e) TF3 and (f) TF4.

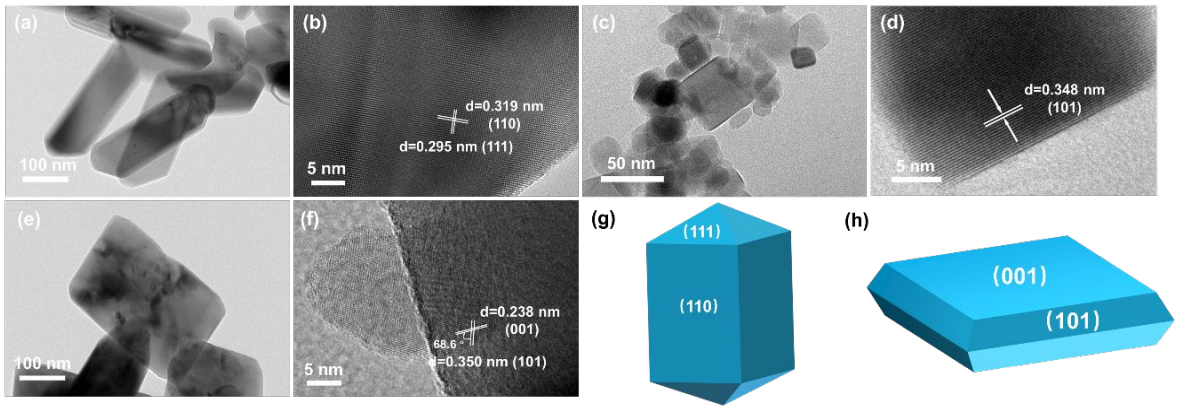

Fig. 3. TEM images of (a) TF0, (c) TF1 and (e) TF4 samples and corresponding HRTEM images (b, d, f), respectively; the schematic illustration of TiO_2 nanorods (g) and TiO_2 nanosheets (h).

More details of TiO_2 samples are determined by TEM. As shown in Fig. 3a, the length and diameter of TiO_2 nanorods (TF0) is around 300 nm and 100 nm, respectively. In the HRTEM image (Fig. 3b), the lattice spacing of 0.319 nm, corresponding to (110) planes, further confirms the rutile phase of TiO_2. It can be inferred that TiO_2 nanorods prepared in this study are exposed large (110) and small (111) facets and the schematic illustration of rutile TiO_2 facets is shown in Fig. 3g. Fig. 3c shows TEM image of TF1 sample which is consisted of well-defined nanosheets with a side size of about 50 nm. The lattice spacing of 0.348 nm can be obtained from Fig. 3d, which corresponds to the (101) planes of anatase TiO_2. As clearly seen in Fig. 3e, the side size of TF4 sample is much larger than that of TF1 sample. The crystal plane of 0.238 nm and 0.350 nm can be observed in Fig. 3f, which confirms the exposed (001) facets and (101) facets of anatase TiO_2 nanosheets. In addition, an angle of 68.6° is obviously observed, which is consistent with the theoretical value for the angle between (001) facets and (101) facets of anatase TiO_2 [28]. The schematic illustration of anatase TiO_2 facets is shown in Fig. 3h. Notably, it is found that the percentage of exposed (001) facets on the TiO_2 nanosheets increases with increasing of HF addition. The TEM results are in good agreement with SEM results. According to the previous study [29], anatase TiO_2 with co-exposed (001) facets and (101) facets can be obtained by adding HF only during the hydrothermal process. In this work, TiO_2 nanosheets were prepared in a mixture of HF and HCl. For TF1 sample, only 1 mL of HF was added while the addition of HCl was 3 mL. The result reveals that fluorine ions play a key role in the formation of TiO_2 nanosheets with exposed (001) facets in the co-existence of HF and HCl, instead of chloride ions.

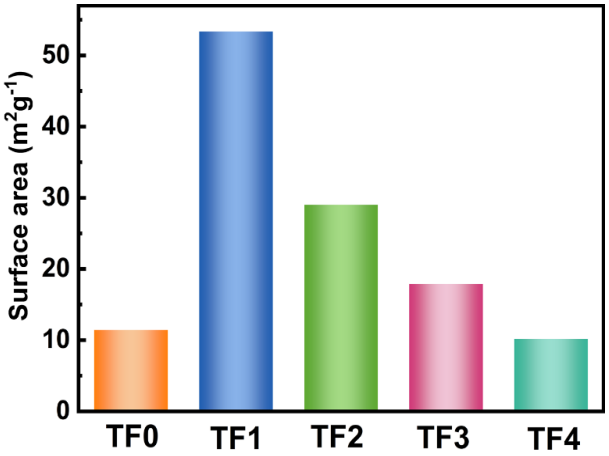

Fig. 4. The specific surface area of various samples.

The BET specific surface area of different TiO_2 samples has been measured and the result is shown in Fig. 4. Owing to the nanosheet structure, TF1 sample shows the largest specific surface area of 53.3 $m^2 \cdot g^{-1}$. With further increase in HF, the surface area of TF4 sample decreases to 10.2 $m^2 \cdot g^{-1}$. As expected, the specific surface area of TF0 sample is smaller, which matches well with XRD and SEM results.

3.3. XPS analysis

XPS measurement was used to investigate the surface chemical composition of the samples. The XPS spectra of TF1 sample prepared in the presence of 1 ml HF and 3 ml HCl are demonstrated in Fig. 5. The full survey XPS spectrum (Fig. 5a) indicates that TF1 sample is mainly composed of Ti, O, and N elements. From the XPS spectra of Ti 2p in Fig. 5b, the two peaks at binding energy of 464.3 and 458.6 eV are assigned to Ti $2p_{1/2}$ and Ti $2p_{3/2}$, respectively, revealing the existence of Ti^{4+} in anatase TiO_2. As shown in Fig. 5c, the O 1s spectra can be divided into three peaks at the binding energy of 532.5, 530.7 and 529.8 eV, which are ascribed to surface hydroxyl group (O–H), O–N bond and Ti–O bond in TiO_2 [30]. The high-resolution spectra of N 1s (Fig. 5d) can be deconvoluted into three peaks at 402.5, 399.5 and 396.3 eV. The first peak may be attributed to the molecularly chemisorbed N species on the sample surface [31]. The characteristic peak of N 1s at 399.5 eV corresponds to the interstitial N atoms in TiO_2 lattice in the form of Ti–O–N while the peak at 396.3 eV is associated with the Ti–N bond as a result of substitutional nitrogen in the TiO_2 lattice [32, 33]. The above XPS results clarify the successful doping of nitrogen into TiO_2.

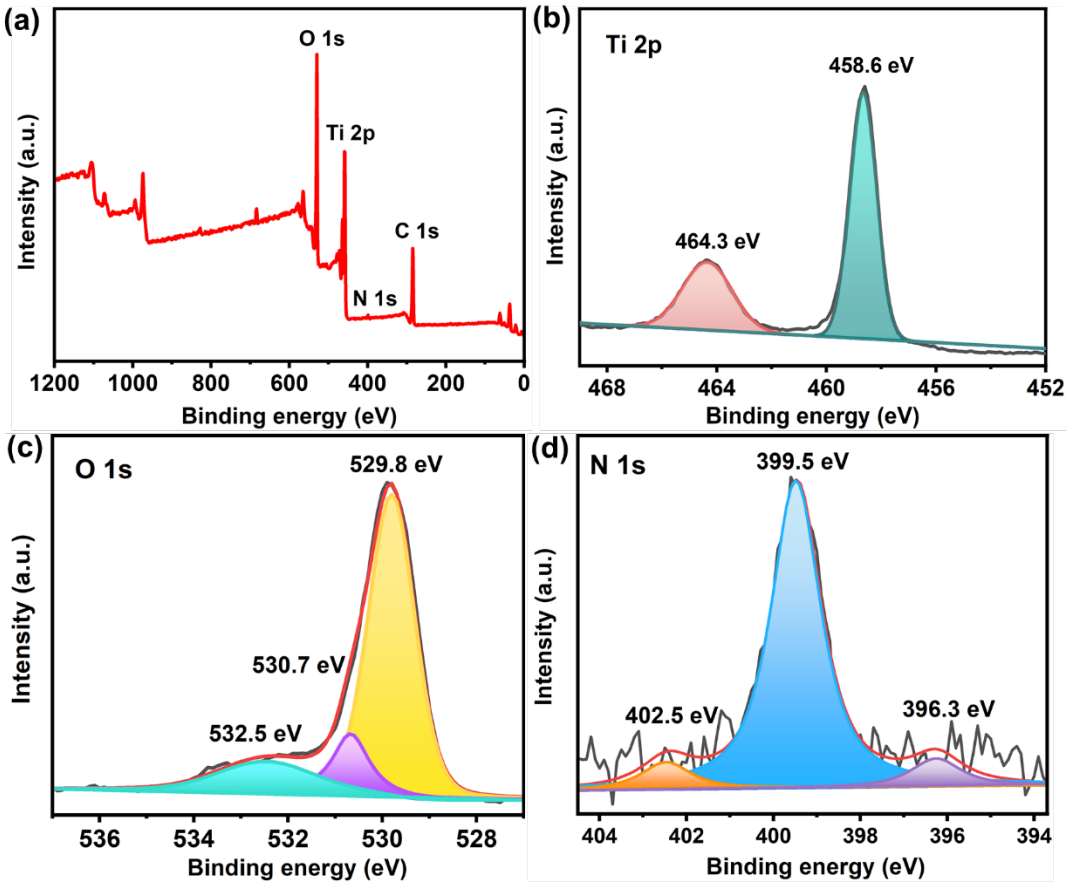

Fig. 5. XPS spectra of TF1 sample: (a) survey spectrum, (b) Ti 2p, (c) O 1s, and (d) N 1s.

3.4. Optical properties and photocatalytic performance

The optical properties of the catalysts can be characterized by UV-vis diffuse reflectance spectra. As can be seen in Fig. 6, the HF addition has little influence on the energy band of TiO_2 and the optical absorption edge of samples is around 410 nm, which indicates that N doping is an effective method to extend light absorption of TiO_2.

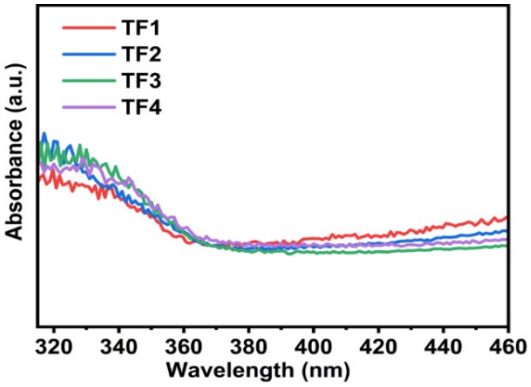

Fig. 6. UV-visible diffuse reflectance spectra of TiO_2 samples prepared with various HF contents.

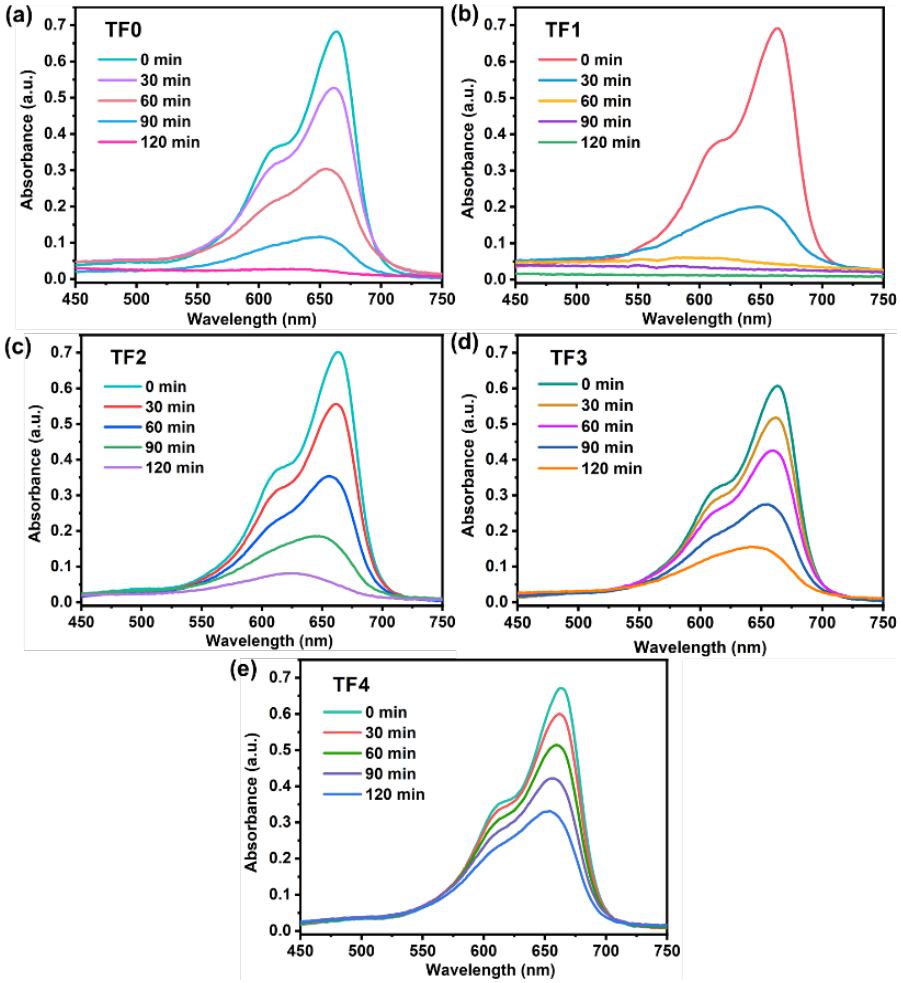

Fig. 7. UV-vis absorption curves of MB dye over the TiO_2 prepared with different HF volumes: (a)TF0, (b)TF1, (c) TF2, (d) TF3, (e) TF4.

The photocatalytic activity of N-doped TiO_2 samples were investigated by degradation MB dye. The UV-vis absorption spectra of MB dye versus irradiation time are illustrated in Fig. 7. It is clear the absorbance of MB decreases gradually with the increase of irradiation time, suggesting the removal of MB dye. It is worth to notice that the MB has been nearly degraded after 60 min when the sample prepared with 1 ml HF and 3 ml HCl.

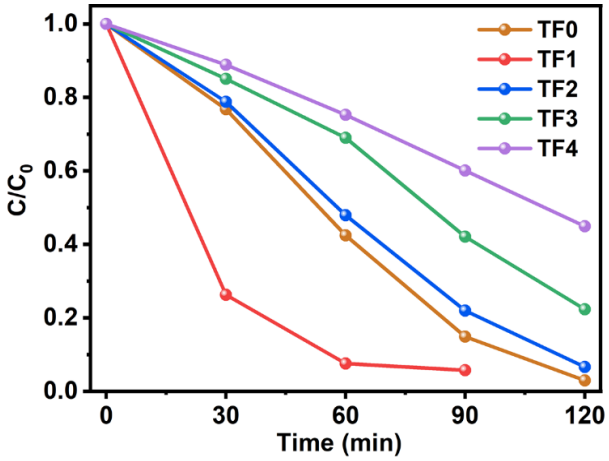

Fig. 8. Comparison of photocatalytic activity of TiO_2 prepared by different HF additions.

Fig. 8 compares the photocatalytic efficiency of N-doped TiO_2 samples. TF1 sample exhibits the highest degradation efficiency of 100% within 90 min and the removal efficiency decreases gradually with the increase of the volume of HF. After 2 h irradiation, the MB decolorization efficiency of TF2, TF3 and TF4 catalysts is 88.5%, 73.1% and 50.7% respectively. The superior photocatalytic activity is attributed to exposed (001) crystal plane of N-doped TiO_2 nanosheets. Moreover, the photocatalytic efficiency follows the trend of specific surface area. The higher surface area can provide more surface active sites for the adsorption of reactant molecules [34], resulting in the improvement of removal rate. For comparison, the photocatalytic performance of TF0 sample is also tested. After irradiation of 120 min, 94.2% of MB can be removed, which indicates that rutile TiO_2 with exposed (110) facets in this work demonstrates excellent photocatalytic activity.

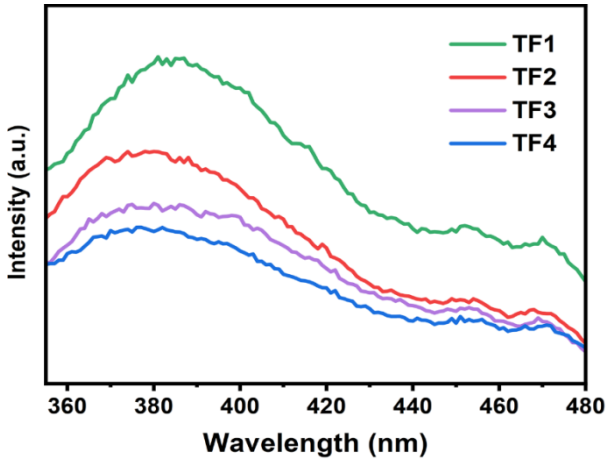

Fig. 9. PL spectra of TiO_2 samples synthesized with various HF additions.

Photoluminescence spectroscopy is usually used to explore the separation efficiency of photogenerated charge carriers of semiconductor materials. Fig. 9 shows the PL signals of N-doped TiO_2 samples with different HF contents excited at 320 nm. In general, the PL intensity strongly depends on the recombination rate of photogenerated electron-hole pairs and the lower PL intensity implies the lower recombination rate of charge carriers and the higher photocatalytic activity of catalysts. It is obvious that the intensity of fluorescence emission peak decreases gradually with increasing HF content. However, the MB degradation efficiency of N-doped TiO_2 samples decreases with increasing HF addition while the PL intensity becomes weaker in this study. These incompatible results may be ascribed to the decreased particle size and the quantum confinement effect [35]. Therefore, an appropriate amount of F ions can significantly reduce the recombination rate of photoinduced electron-hole pairs in TiO_2 and the particle size plays an important role in the charge separation efficiency.

3.5. Mechanism of photocatalytic degradation

In order to further explore the photocatalytic mechanism of N-doped TiO_2 nanosheets, the band structure of TF1 is analyzed. According to the UV-vis DRS (Fig. 6), the bandgap of the sample can be calculated by the following formula [36]:

$$ah\upsilon = A\left(h\upsilon - E_g\right)^2$$

where α, h, v, A, and Eg represent absorption coefficient, Planck constant, light frequency, a constant and bandgap energy, respectively. The estimated bandgap energy of TF1 is 3.01 eV, a little smaller than pure TiO_2 of 3.2 eV [37], which is due to the introduction of N that narrows the bandgap of TiO_2, leading to higher light harvest capacity.

The valence band (VB) of the TF1 is measured by X-ray photoelectron spectroscopy and the VB value is 2.60 eV (Fig. 10b). The final VB position versus normal hydrogen electrode (NHE) can be calculated by the following formula [38]:

$$E_{NHE} = \Phi + E_{VL} - 4.44$$

where $E_{NHE,}$ Φ and E_{VL} are the potential of normal hydrogen electrode, electron work function of the instrument (4.6 eV) and the potential of vacuum level, respectively. Consequently, the actual VB potential of TF1 can be determined as 2.76 eV. Thus, the conduction band (CB) value of -0.25 eV is obtained. The band structure and the photocatalytic degradation mechanism are illustrated in Fig. 10c.

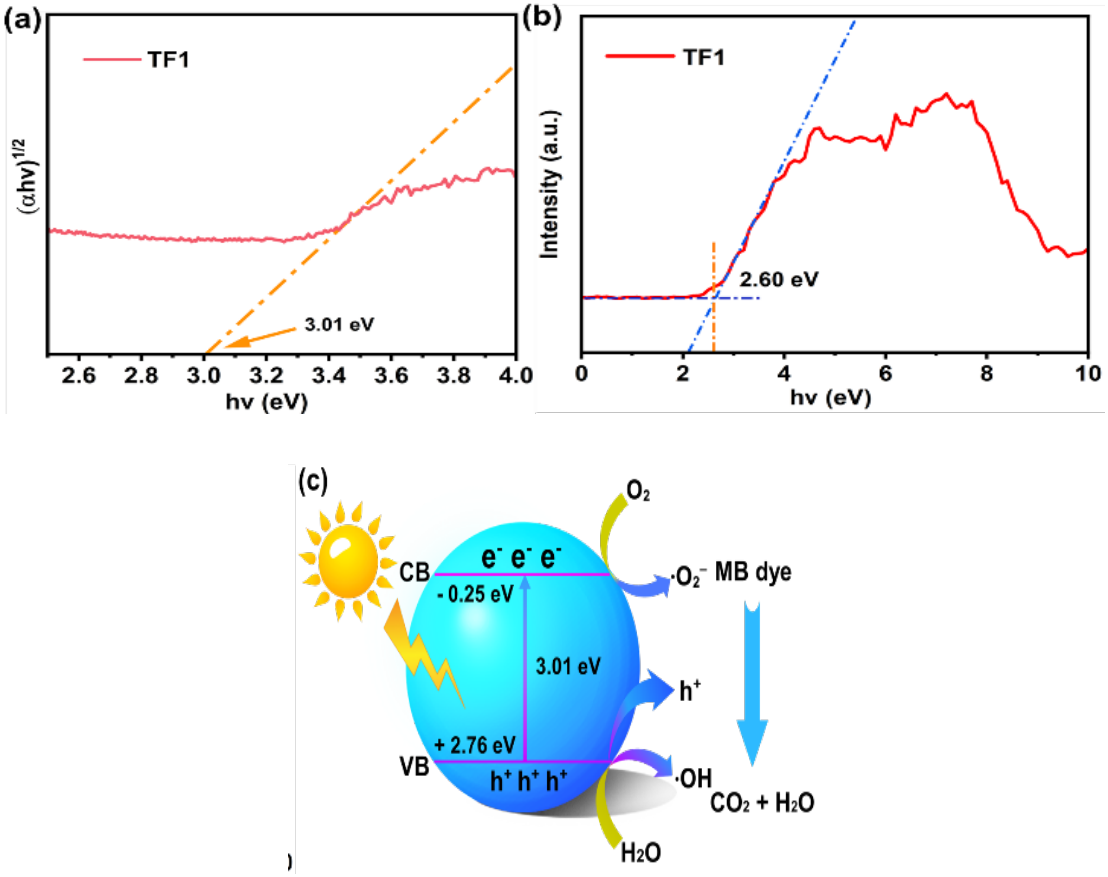

Fig. 10. (a) bandgap and (b) XPS valence band of TF1 catalyst; (c) photocatalytic degradation mechanism of MB dye.

The potential of CB is more negative, then the photogenerated electrons in the CB could reduce O_2 to $\cdot O_2^-$ radicals. Meanwhile, the VB potential is more positive than the standard oxidation potential of $H_2O/\cdot OH$ (+2.72 eV vs. NHE), thus generating ·OH radicals [39]. Additionally, a part of holes in the VB may directly oxidize MB dye. Hence, the N-doped TiO_2 nanosheets not only promote the separation and transfer of photogenerated electron-hole pairs, but also maintain the strong redox ability in the photocatalytic reaction, which is suitable for the decomposition of MB dye.

4. Conclusion

N-doped TiO_2 nanosheets with a high percentage of exposed (001) facets were synthesized by one step hydrothermal method using TiN as precursor in the presence of HCl and HF. The results showed that fluorine ions can affect the crystal structure, grain size and surface morphology and the photocatalytic performance of TiO_2. The MB removal efficiency decreased with increasing HF addition. When the proportion of HF and HCl was 1:3, MB dye could be completely degraded by TiO_2 nanosheets within 90 min due to larger specific surface area. This

work provides a new route for the syntheses of N-doped TiO_2 nanosheets with higher photocatalytic activity.

Acknowledgements

This work was supported by National Natural Science Foundation of China (No. 51702027).

References

[1] D. J. Chen, Y. L. Cheng, N. Zhou, P. Chen, Y. P. Wang, K. Li, S. H. Huo, P. F. Cheng, P. Peng, R. C. Zhang, L. Wang, H. Liu, Journal of Cleaner Production 268, 121725 (2020); https://doi.org/10.1016/j.jclepro.2020.121725
[2] V. Kumaravel, S. Mathew, J. Bartlett, S. C. Pillai, Applied Catalysis B: Environmental 244, 1021-64 (2019); https://doi.org/10.1016/j.apcatb.2018.11.080
[3] E. I. Cedillo-González, R. Riccò, M. Montorsi, M. Montorsi, P. Falcaro, C. Siligardi, Building and Environment 71,7-14 (2014); http://dx.doi.org/10.1016/j.buildenv.2013.09.007
[4] J. Schneider, M. Matsuoka, M. Takeuchi, J. Zhang, Y. Horiuchi, M. Anpo, D. W. Bahnemann, Chemical Reviews 114, 9919-86 (2014); http://dx.doi.org/10.1021/cr5001892
[5] Q. R. Zhao, S. Y. Chen, B. H. Ren, S. N. Liu, Y. C. Zhang, X. Luo, W. Feng, Y. Sun, Optical Materials 135, 113266 (2023); https://doi.org/10.1016/j.optmat.2022.113266
[6] K. H. Leong, H. Y. Chu, S. Ibrahim, P. Saravanan, Beilstein Journal of Nanotechnology 6, 428-37 (2015); https://doi.org/10.3762/bjnano.6.43
[7] C. Gao, T. Wei, Y. Zhang, X. Song, Y. Huan, H. Liu, M. Zhao, J. Yu, X. Chen, Advanced Materials 31, 1806596 (2019); https://doi.org/10.1002/adma.201806596
[8] Y. Li, J. Liu, Z. Jia, Materials Letters 60 (13-14), 1753-1757 (2006); https://doi.org/10.1016/j.matlet.2005.12.012
[9] Y. Jun, M. F. Casula, J. Sim, S. Y. Kim, J. Cheon, A. P. Alivisatos, Journal of the American Chemical Society 125 (51), 15981-15985 (2003); https://doi.org/10.1021/ja0369515
[10] J. Zhang, Y. Zhang, Y. Lei, C. Pan, Catalysis Science & Technology 1 (2), 273-278 (2011); https://doi.org/10.1039/c0cy00051e
[11] Y. Yu, C. Cao, W. Li, P. Li, J. Qu, W. Song, Nano Research 5, 434-42 (2012); https://doi.org/10.1007/s12274-012-0226-1
[12] J. Qu, Y. Wang, X. Mu, J. Hu, B. Zeng, Y. Lu, M. Sui, R. Li, C. Li, Advanced Materials 34 (37), 2203320 (2022). https://doi.org/10.1002/adma.202203320
[13] Z. Lyu, B. Liu, R. Wang, L. Tian, Journal of Materials Research and Technology 32 (14), 2781-2789 (2017). https://doi.org/10.1557/jmr.2017.232
[14] H. G. Yang, C. H. Sun, S. Z. Qiao, J. Zou, G. Liu, S. C. Smith, H. M. Cheng, G. Q. Lu, Nature 453 (7195), 638-641 (2008); https://doi.org/10.1038/nature06964
[15] Z. Zheng, B. Huang, X. Qin, X. Zhang, Y. Dai, M. Jiang, P. Wang, M. Whangbo, Chemistry - A European Journal 15 (46), 12576-12579 (2009); https://doi.org/10.1002/chem.200902438
[16] Y. Wang, H. Zhang, Y. Han, P. Liu, X. Yao, H. Zhao, Chemical Communications 47 (10), 2829–2831 (2011); https://doi.org/10.1039/c0cc04848h
[17] Q. Xiang, J. Yu, Chinese Journal of Catalysis 32 (3-4), 525-531 (2011); https://doi.org/10.1016/S1872-2067(10)60186-6
[18] L. Chu, Z. Qin, J. Yang, X. A. Li, Scientific Reports 5 (1) (2015). https://doi.org/10.1038/srep12143
[19] Y. Qin, Z. Wang, J. Jiang, L. Xing, K. Wu, Chemical Engineering Journal 394, 124917 (2020); https://doi.org/10.1016/j.cej.2020.124917
[20] M. Dozzi, E. Selli, Catalysts 3 (2), 455-485 (2013); https://doi.org/10.3390/catal3020455.

[21] K. Lv, J. Yu, L. Cui, S. Chen, M. Li, Journal of Alloys and Compounds 509 (13), 4557-4562 (2011); https://doi.org/ 10.1016/j.jallcom.2011.01.103
[22] Y. Luan, L. Jing, Q. Meng, H. Nan, P. Luan, M. Xie, Y. Feng, The Journal of Physical Chemistry C 116 (32), 17094-17100 (2012); https://doi.org/10.1021/jp305142j
[23] Q. J. Xiang, K. Lv, J. G. Yu, Applied Catalysis B: Environmental 96 (3-4), 557-564 (2010); https://doi.org/10.1016/j.apcatb.2010.03.020
[24] L. Dong, K. Cheng, W. Weng, C. Song, P. Du, G. Shen, G. Han, Thin Solid Films 519 (15), 4634-4640 (2011); https://doi.org/ 10.1016/j.tsf.2011.01.008
[25] A. O. Bokuniaeva, A. S. Vorokh, Journal of physics. Conference series 1410 (1), 012057 (2019); https://doi.org/10.1088/1742-6596/1410/1/012057
[26] Y. Yang, L. Luo, M. Xiao, H. Li, X. Pan, F. Jiang, Materials Science in Semiconductor Processing 40, 183-193 (2015); http://dx.doi.org/10.1016/j.mssp.2015.06.012
[27] X. Xia, S. Peng, Y. Bao, Y. Wang, B. Lei, Z. Wang, Z. Huang, Y. Gao, Journal of Power Sources 376, 11-17 (2018); https://doi.org/10.1016/j.jpowsour.2017.11.067
[28] G. Liu, C. Sun, H. G. Yang, S. C. Smith, L. Wang, G. Q. M. Lu, H. Cheng, Chemical Communications 46 (5), 755-757 (2010); https://doi.org/10.1039/b919895d
[29] H. Yin, Y. Wada, T. Kitamura, S. Kambe, S. Murasawa, H. Mori, T. Sakata, S. Yanagida, Journal of Materials Chemistry 11 (6), 1694-1703 (2001); https://doi.org/10.1039/b008974p
[30] M. Chi, X. Sun, A. Sujan, Z. Davis, B. J. Tatarchuk, Fuel 238, 454-461 (2019); https://doi.org/10.1016/j.fuel.2018.10.114
[31] G. Yang, Z. Jiang, H. Shi, T. Xiao, Z. Yan, Journal of Materials Chemistry 20 (25), 5301 (2010); https://doi.org/10.1039/c0jm00376j
[32] T. Zhang, A. Ni, Y. Xu, D. Fu, P. Lin, Journal of Physics and Chemistry of Solids 170, 110923 (2022); https://doi.org/10.1016/j.jpcs.2022.110923
[33] Y. Yang, X. Yang, Q. Jia, S. Zheng, Z. Lin, Z. Qin, Vacuum 207, 111577 (2023); https://doi.org/10.1016/j.vacuum.2022.111577
[34] C. Liu, Y. Qin, W. Guo, Y. Shi, Z. Wang, Y. Yu, L. Wu, Applied Surface Science 580, 152262 (2022); https://doi.org/10.1016/j.apsusc.2021.152262
[35] X. Xue, W. Ji, Z. Mao, H. Mao, Y. Wang, X. Wang, W. Ruan, B. Zhao, J. R. Lombardi, The Journal of Physical Chemistry C 116 (15), 8792-8797 (2012); https://doi.org/10.1021/jp2122196
[36] L. E. McNeil, R. H. French, Acta Materialia 48 (18-19), 4571-4576 (2000); https://doi.org/10.1016/S1359-6454(00)00243-3
[37] R. C. Zulkifli, F. Azaman, M. H. Razali, A. Ali, M. A. A. M. Nor, Digest Journal of Nanomaterials and Biostructures 18 (1), 243-252 (2023); https://doi.org/10.15251/DJNB.2023.181.243
[38] Q. Zhao, S. Liu, S. Chen, B. Ren, Y. Zhang, X. Luo, Y. Sun, Chemical Physics Letters 805, 139908 (2022); https://doi.org/10.1016/j.cplett.2022.139908
[39] J. Cheng, X. Liu, J. A. Kattirtzi, J. VandeVondele, M. Sprik, Angewandte Chemie 126 (45), 12242-12246 (2014); https://doi.org/10.1002/ange.201405648